DOI: 10.1002/ejic.201001095

Synthesis of Heterobimetallic Zn/Co Carbamates: Single-Source Precursors of Nanosized Magnetic Oxides Under Mild Conditions

Dan Domide,[a] Olaf Walter,[b] Silke Behrens,[b] Elisabeth Kaifer,[a] and Hans-Jörg Himmel*[a]

Keywords: Cobalt / Zinc / Nanostructures / Heterobimetallic complexes / Carbamates

Tetrameric Zn alkyl carbamates $[ZnR(O_2CNR'_2)]_4$ (R = Me or Et, R′ = *i*Pr) have been synthesized from alkylzinc amides and CO_2. The reaction of these carbamates with specially designed Co^{II} complexes afforded new heterobimetallic (Zn/Co) carbamate complexes. The thermal decomposition of these single-source precursors under mild conditions (200–300 °C) led to magnetic mixed-metal oxide nanoparticles. Two phases were identified that are isostructural with ZnO (wurtzite phase) and CoO (cubic rock salt structure), but both contain Zn and Co in varying molar ratios. The particles with the ZnO-type structure have a mean average size of 7.7 nm, whereas the particles with the CoO-type structure are much larger (ca. 48 nm).

Introduction

ZnO nanoparticles are of interest as they have a variety of applications. ZnO is a wide band gap semiconductor (3.37 eV at room temperature). The emission spectra of ZnO nanoparticles have been intensively studied[1] and display luminescent properties in the near ultraviolet and visible regions. The possible application of ZnO in dye-sensitized solar cells[2] as a replacement for the currently favoured TiO_2 is unfortunately still hampered by its instability in acidic dye solutions,[3,4] leading to Zn^{II}–dye complexes or agglomerates. However, ZnO nanocrystallites have recently been shown to exhibit high conversion efficiency,[5] and coating of the ZnO particles to yield core–shell structures can improve their stability. Hence, despite the instability caused by the relatively small Zn–O bond energy in ZnO relative to the Ti–O bond energy in TiO_2, research into ZnO nanoparticles in this field is continuing. In particular, TiO_2-coated ZnO nanowire arrays seem to be highly efficient. Some of the various ways to obtain ZnO nanoparticles rely on coordination and organometallic compounds as precursors. The precursors include dialkylzinc compounds like $ZnCy_2$ (Cy = c-C_6H_{11}) or $ZnEt_2$,[6,7] tetranuclear alkoxide complexes of the general formula $[ZnR(OR')]_4$ (R, R′ = alkyl, e.g., R = Me and R′ = *i*Pr or *t*Bu),[8] salts of cationic complexes like $[Zn_4(LH)_4]^{4+}$ (with LH_2 = bipyridinediol)[9] and also tetrameric Zn carbamato complexes $[ZnR(O_2CNR'_2)]_4$ (e.g., R = Et, R′ = *i*Pr)[10] or $[Zn_4O(O_2CNR_2)_6]$ (R = Et, chemical vapour deposition).[11] $Zn_xMg_{1-x}O$ thin films were recently fabricated using mixed-metal ZnMg carbamates.[12]

Clearly, alloy oxides containing transition metals with unpaired electrons are also of considerable interest, for example, for the fabrication of magnetic and optoelectronic devices.[13–15] Hence oxides such as $Zn_{1-x}Co_xO$ (x usually being much smaller than 1) represent magnetic semiconductors and the control over x allows "band-gap and spin engineering".[16] Several methods (including solid-state reactions at high temperatures, hydrolysis of ionic salts in an aqueous solution or an organic polyol, and then often in combination with various film-producing techniques such as sol-gel dip-coating or spray pyrolysis, or decomposition of organometallic precursors in aqueous solutions) have been developed to gain access to these mixed oxides. Still challenging but important for a number of applications is the synthesis of nanosized particles with diameters in the range of not more than several nanometers and narrow size distribution. Recently, Polarz and Driess et al. reported a method for the synthesis of heterobimetallic tetranuclear alkoxide complexes that decompose thermally under relatively mild conditions ($T \geq 250$ °C) to give nanosized two-component magnetic oxides.[9] It was shown that the average diameter of the particles can be relatively easily controlled by the decomposition temperature. In the first instance mixtures of precursor clusters were obtained in which one, two or three Zn atoms of a tetranuclear Zn compound with a heterocubane-type structure are replaced by Co, Ni or Mn atoms. These clusters had to be purified in a second step prior to decomposition to the alloy oxides.

[a] Anorganisch-Chemisches Institut, Ruprecht-Karls-Universität Heidelberg,
Im Neuenheimer Feld 270, 69120 Heidelberg, Germany
Fax: +49-6221-545707
E-mail: hans-jorg.himmel@aci.uni-heidelberg.de
[b] Institut für Katalyseforschung und -technologie (IKFT), Karlsruher Institut für Technologie (KIT), Campus Nord, Postfach 3640, 76021 Karlsruhe, Germany
Supporting information for this article is available on the WWW under http://dx.doi.org/10.1002/ejic.201001095.

We report herein the fabrication of nanosized magnetic semiconductor materials using single-source molecular organometallic precursors. First, CO_2 was allowed to react with an alkylzinc amide to give an oligonuclear carbamate, which was treated in a second step with a Co^{II} compound to give a tetrameric precursor complex. Its thermal decomposition under mild conditions led to nanosized alloy oxide materials. The oxygen in these oxides stems exclusively from CO_2 and the method can presumably be extended to introduce a number of transition metals into the ZnO nanoparticles.

Results and Discussion

The reaction of [ZnRN(*i*Pr)$_2$] [or a R_2Zn/HN(*i*Pr)$_2$ mixture; R = Me or Et] with CO_2 to give the tetranuclear complex [ZnR{O_2CN(*i*Pr)$_2$}]$_4$, **1-Me** or **1-Et**, has been reported previously.[10,17] These carbamates are easy to synthesize in high yields and were therefore used in the next step of the precursor synthesis. We[18,19] and others[20] have previously shown that N-bases can break up these tetrameric carbamate units to give (depending on the reaction conditions and the specific base) tri-, bi- or mononuclear carbamates. Therefore our initial idea was to attach an N-base to the neutral ligands L in Co^{II} halide complexes with the general formula [L_2CoCl_2]. To this end we synthesized three different $CoCl_2$ complexes and tested their reaction with the tetrameric carbamate, namely the tetrahedral complexes [$CoCl_2$(map)$_2$] (**2**; map = 2-(methylamino)pyridine) and [$CoCl_2$(maep)] {**3**; maep = 2-[2-(methylamino)ethyl]-pyridine} as well as the octahedral complex [$CoCl_2$-(maep)$_2$] (**4**; see Scheme 1). The crystal structures of these three complexes, which have not been reported thus far, are shown in Figure 1. In complexes **3** and **4**, but not in **2**, the amino arms of the pyridine ligands coordinate to the Co atom. An interesting and possibly important structural detail to appreciate the reactivity (see the discussion below) is the presence of H···Cl bonding in **2**, which might assist cleavage of the Co–Cl bonds in the course of the following reactions. The longest Co–Cl bond, however, was found in the octahedral complex **4** [247.78(6) pm vs. 224.93(6)/224.35(6) pm in **2** and 223.40(8)/224.88(10) pm in **3**].

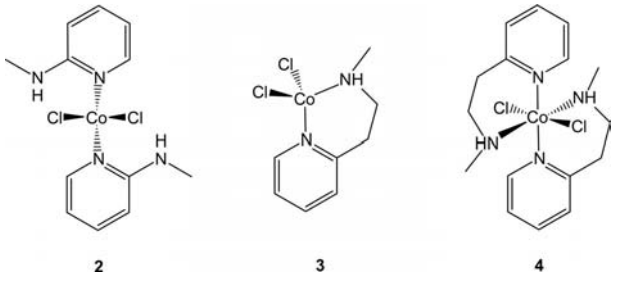

Scheme 1.

Complexes **3** and **4** showed no sign of reaction with **1-Et** or **1-Me**. On the other hand, the reaction of complex **2** with **1-Et** in toluene yielded a new Co- and Zn-containing, intensely purple-coloured product **5-Et** in 34% yield. The UV/Vis spectrum of a solution of **5-Et** in toluene is displayed in Figure 2a together with that of **2**. The UV/Vis spectra of both **2** and **5-Et** feature three absorptions with maxima at 15640, 16100 and 17100 cm^{-1} for **2** and at around 16200, 16900 and 18200 cm^{-1} for **5-Et**. The spectrum of **5-Et** can also be compared with that obtained previously for the Co carbamate complex [Co{O_2C-(NEt$_2$)$_2$}]$_6$[21] and proves the presence of Co atoms in the product **5-Et**. Atom absorption spectrometry (AAS) as well as inductively coupled plasma mass spectrometry (ICP-MS) analyses returned an average Zn/Co molar ratio of 2.5:1.5 for **5-Et**. Crystals of **5-Et** were grown from toluene at –20 °C. The X-ray diffraction analysis of these crystals (see Figure 3) showed the presence of tetranuclear clusters with the general formula [M_4Et_2{O_2CN(*i*Pr)$_2$}$_6$] (M = Co or Zn atoms) in which the four metal ions are connected through bridging carbamate units.

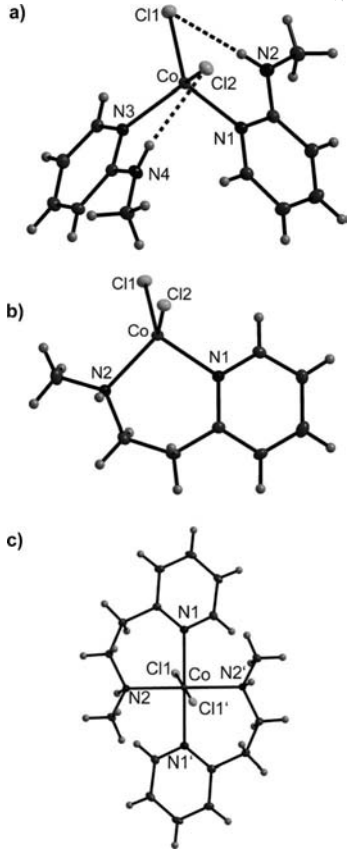

Figure 1. Molecular structures of a) **2**, b) **3** and c) **4** as derived from single-crystal X-ray diffraction. Hydrogen atoms have been omitted for the sake of clarity. Thermal ellipsoids are drawn at the 50% probability level. Selected bond lengths [pm] and bond angles [°] for **2**: Co–Cl1 224.93(6), Co–Cl2 224.35(6), Co–N1 204.86(14), Co–N3 204.21(14), N2···Cl1 325.3(3), N2–H···Cl1 244.9(3), N4···Cl2 329.8(3), N4H···Cl2 251.1(3), Cl1–Co–Cl2 113.67(2), N1–Co–N3 102.36(5). Selected bond lengths [pm] and bond angles [°] for **3**: Co–Cl1 223.40(8), Co–Cl2 224.88(10), Co–N1 203.4(2), Co–N2 204.2(2), Cl1–Co–Cl2 118.38(3), N1–Co–N2 100.11(9). Selected bond lengths [pm] and bond angles [°] for **4**: Co–Cl1 247.78(6), Co–N1 223.69(16), Co–N2 217.94(16), N1–Co–N2 88.73(6), N1–Co–Cl1 93.50(4), N2–Co–Cl1 89.36(4).

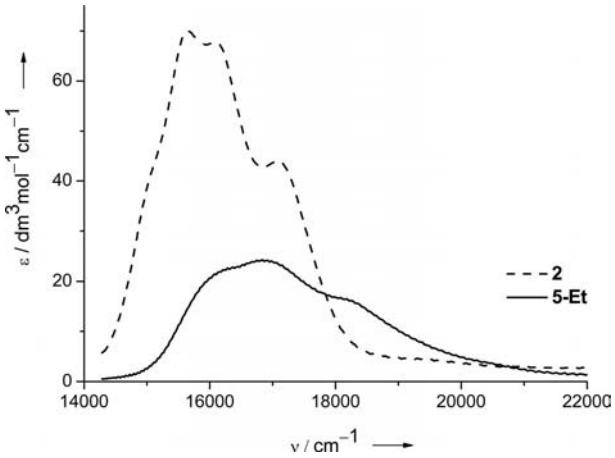

Figure 2. UV/Vis spectrum of **5-Et** in toluene. For comparison, the UV/Vis spectrum of the starting Co complex **2** is also displayed.

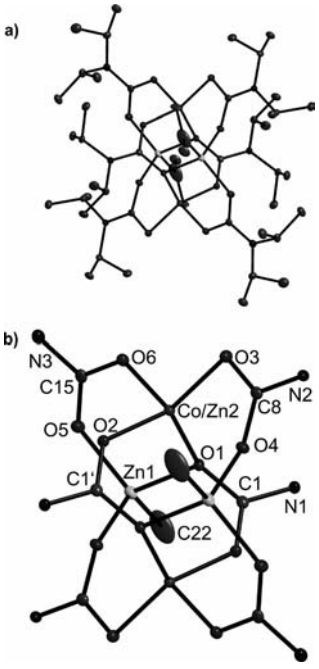

Figure 3. Molecular structure of **5-Et**. a) Hydrogen atoms have been omitted for the sake of clarity. b) Isopropyl groups have been omitted. Of the ethyl groups, only the methylene C atom is shown. Thermal ellipsoids are drawn at the 50% probability level. Selected bond lengths [pm] and bond angles [°]: Zn1–O1 207.56(19), Zn1–O4′ 203.2(2), Zn1–O5 194.3(2), Zn1–C22 205.9(2), Co/Zn2–O1 199.5(2), Co/Zn2–O2 195.5(2), Co/Zn2–O3 198.78(19), Co/Zn2–O6 196.3(2), O1–C1 132.1(3), O2–C1′ 126.1(3), O3–C8 127.6(4), O4–C8 129.4(3), O5–C15 127.5(3), O6–C15 128.0(3), N1–C1 133.3(4), N2–C8 134.5(4), N3–C15 135.0(4), O1–Zn1–O4′ 93.33(8), O5–Zn1–C22 125.34(11), O2–Co/Zn2–O3 120.52(9), O1–Co/Zn2–O6 97.74(9), O1–C1–O2′ 121.4(3), O3–C8–O4 118.1(3), O5–C15–O6 123.8(3).

All four metal ions are tetrahedrally coordinated. As anticipated, it was not possible to distinguish unambiguously between Zn and Co atoms purely on the basis of the structure derived from the X-ray diffraction analysis. Two of the metal ions carry terminal ethyl ligands and were therefore tentatively assigned to Zn. Because the ethyl groups were attached to Zn atoms in the reactant **1-Et**, it is likely that these groups are also attached to Zn atoms in the product **5-Et**. On the basis of the AAS studies, in half of the complexes the two remaining metal sites are occupied by Co and in the other half by one Zn and one Co. Thus, the crystal should consist of an equimolar mixture of the two complexes $[Zn_2Co_2Et_2\{O_2CN(i\text{Pr})_2\}_6]$ and $[Zn_3CoEt_2\{O_2CN(i\text{Pr})_2\}_6]$. For the two sites that are occupied either by Zn or Co atoms, the metal–oxygen bond lengths fall into the range 195.5(2)–199.5(2) pm. The variation in the EtZn–O bond lengths is larger [194.3(2)–207.56(2) pm]. Moreover, the refinement of the X-ray diffraction data points to the presence of around 0.25% of chloride in the place of ethyl ligands. The overall formula of **5-Et** then is $C_{58.8}H_{107}Cl_{0.6}Co_{1.5}N_6O_{12}Zn_{2.5}$. It will be shown below that these chloride "contaminations" did not affect the quality of the oxide particles grown by decomposition of **5-Et**. In another series of experiments we synthesized **5-Me** (similar to **5-Et**, but with Me groups instead of Et groups) by the reaction of $[ZnMe\{O_2CN(i\text{Pr})_2\}]_4$ with **1-Me** and **2**.[22] Crystals suitable for an XRD analysis were grown from toluene. Two slightly different complexes were found within the unit cell. As anticipated, the molecular structure is similar to that of **5-Et**. Figure 4 displays the structure of one of the two complexes. The Co/Zn–O bond lengths are in the range 196.63(18)–201.20(17) pm. Again, the variation in MeZn–O distances is larger [192.97(17)–207.14(18) pm].

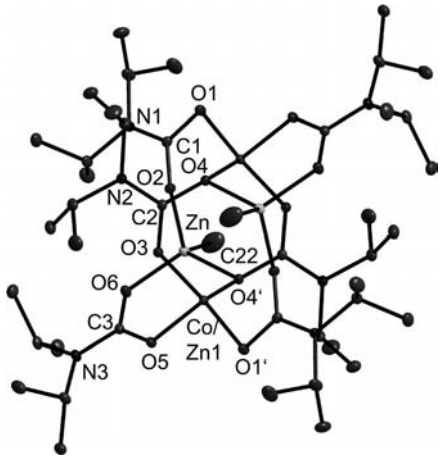

Figure 4. Molecular structure of **5-Me**. Hydrogen atoms have been omitted for the sake of clarity. Thermal ellipsoids are drawn at the 50% probability level. Selected bond lengths [pm] and bond angles [°]: Co/Zn1–O1′ 200.92(18), Co/Zn1–O3 196.72(18), Co/Zn1–O4′ 201.20(17), Co/Zn1–O5 196.63(18), Zn–O2 203.10(18), Zn–O4′ 207.14(18), Zn–O6 192.97(19), Zn–C22 208.05(15), O1–C1 127.6(3), O2–C1 129.8(3), O3–C2 125.2(3), O4–C2 131.7(3), O5–C3 127.3(3), O6–C3 127.8(3), N1–C1 133.9(3), N2–C2 134.5(3), N3–C3 135.0(3), O1′–Co/Zn1–O3 118.11(8), O4′–Co/Zn1–O5 96.74(8), O2–Zn–O4′ 93.51(7), O6–Zn–C22 124.84(8).

Superconducting quantum interference device (SQUID) data for complex **5-Et** were also recorded. With 2.35 K cm^3 mol^{-1}, the χT value at 300 K is slightly higher than the spin only value for $1.5N_A$ magnetically non-coupled Co atoms in one mole of substance (2.11 K cm^3 mol^{-1}). The magnetic measurements are thus in line with the results

of the AAS measurements. The χ^{-1} versus T curve shown in Figure 5 (a) follows the Curie–Weiss law above 50 K with a Curie temperature Θ of –16.1 K and a Curie constant C of 0.40 $cm^3\,K\,mol^{-1}$. The negative value of the Curie temperature indicates antiferromagnetic coupling. The form of the χT versus T curve (Figure 5, b) also points to weak magnetic exchange between the Co^{II} ions in **5-Et**.

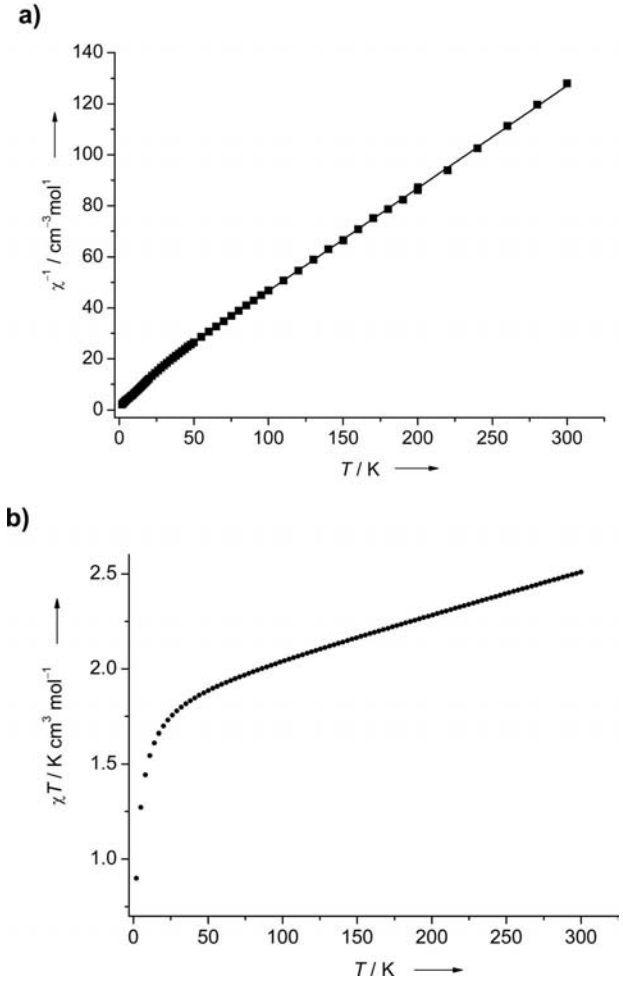

Figure 5. a) χ^{-1} vs. T and b) χT vs. T plots from SQUID measurements (at 500 Oe) of solid **5-Et**.

The complex **5-Et** turned out to be extremely reactive and reacted particularly rapidly with H_2O. From a solution of **5-Et** in CH_3CN the tetranuclear complex $[M_4(\mu_4\text{-}O)\{O_2CN(i\text{Pr})_2\}_6]$ (**6**) crystallized with one oxygen atom at its centre, but with no ethyl groups. As in **5-Et**, the Zn/Co ratio is 2.5:1.5. The unit cell features two slightly different molecules. The molecular structure of one of these molecules is shown in Figure 6 (a). It is similar to $[Zn_4(\mu_4\text{-}O)(O_2CNR_2)_6]$ complexes (e.g., R = Me, Et or *i*Pr) reported previously.[23,24] Interestingly, another carbamate complex crystallized from a solution of **5-Et** in hexane, which turned out to be an octanuclear complex (the dimer of **6**) featuring two oxygen atoms at the centre, namely $[M_8(\mu_4\text{-}O)_2\{O_2CN(i\text{Pr})_2\}_{12}]$ (**7**; M = Zn or Co) with an average Zn/Co ratio of 5:3. The molecular structure is shown in Figure 6 (b). The structure of this complex can be compared directly with that of the Zn complex $[Zn_8(\mu_4\text{-}O)_2\{O_2CN(i\text{Pr})_2\}_{12}]$, which has previously been synthesized.[25] Lamb and co-workers have already reported the isolation of tetra- or octanuclear complexes depending on the solvent used for recrystallization ($[Zn_4(\mu_4\text{-}O)\{O_2CN(i\text{Pr})_2\}_6]$ isolated, for example, from CH_3CN solution and $[Zn_4(\mu_4\text{-}O)\{O_2CN(i\text{Pr})_2\}_6]_2$ isolated from alkane solutions).[25] Thus, it is likely that **7** is formed by the dimerization of **6**. We recorded the high-resolution mass spectrum of complex **6**. The $[M]^+$ group of peaks is shown in Figure 7 together with a simulated pattern including the complexes with four, three, two and one Co atom. It can be seen that complexes with one or two Co atoms, which are present in similar amounts, dominate. Thus, the results are in agreement with the Zn/Co ratio of 2.5:1.5 derived from the AAS measurements for **5-Et**.

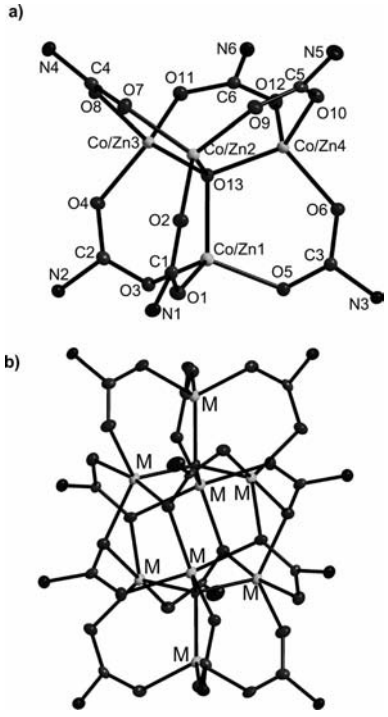

Figure 6. Molecular structures of a) **6** and b) **7** as derived from single-crystal X-ray diffraction. Isopropyl groups have been omitted for the sake of clarity. Thermal ellipsoids are drawn at the 50% probability level. Selected bond lengths [pm] and bond angles [°] for **6**: Co/Zn1–O1 194.9(3), Co/Zn1–O3 193.2(3), Co/Zn1–O5 193.3(3), Co/Zn1–O13 194.5(3), Co/Zn2–O2 194.9(3), Co/Zn2–O7 194.4(3), Co/Zn2–O9 193.7(3), Co/Zn2–O13 194.5(3), Co/Zn3–O4 195.1(3), Co/Zn3–O8 196.5(3), Co/Zn3–O11 195.5(3), Co/Zn3–O13 195.0(3), Co/Zn4–O6 193.6(3), Co/Zn4–O10 195.2(3), Co/Zn4–O12 192.9(3), Co/Zn4–O13 194.1(3), O1–C1 127.1(5), O2–C1 128.0(5), O3–C2 127.8(5), O4–C2 127.6(5), O5–C3 126.8(5), O6–C3 128.2(5), O7–C4 126.9(5), O8–C4 128.0(5), O9–C5 127.7(5), O10–C5 126.9(5), O11–C6 128.5(5), O12–C6 127.0(5), N1–C1 135.7(5), N2–C2 135.8(5), N3–C3 135.4(5), N4–C4 135.3(5), N5–C5 135.3(5), N6–C6 134.9(5), Co/Zn1–O13–Co/Zn2 107.74(12), Co/Zn3–O13–Co/Zn4 109.72(12), O1–C1–O2 124.4(4), O3–C2–O4 124.5(4), O5–C3–O6 124.4(4), O7–C4–O8 124.4(4), O9–C5–O10 125.0(4), O11–C6–O12 123.7(4). In **7**, the Zn/Co atoms are labelled M.

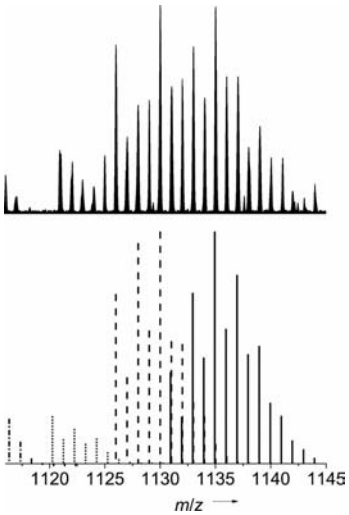

Figure 7. Top: Mass spectrum (FD^+) of compound **6**. Bottom: Simulations of the expected isotopic patterns: dashed-dotted lines: $[Co_4(\mu_4\text{-}O)\{O_2CN(i\text{Pr})_2\}_6]$; dotted lines: $[ZnCo_3(\mu_4\text{-}O)\{O_2CN(i\text{Pr})_2\}_6]$; dashed lines: $[Zn_2Co_2(\mu_4\text{-}O)\{O_2CN(i\text{Pr})_2\}_6]$; solid lines: $[Zn_3Co(\mu_4\text{-}O)\{O_2CN(i\text{Pr})_2\}_6]$.

Subsequently we studied the thermal decomposition of the fully characterized molecular precursor **5-Et**. The TG curves for three different heating rates (2, 5 and 10 °C min^{-1}) are plotted in Figure 8. It can be seen that the compound loses 76% of its initial mass at all rates of heating, in agreement with the theoretical weight loss of 77% for decomposition, to give an oxide with the overall formula $Zn_{2.5}Co_{1.5}O_4$. The process is complete at 205 °C for a heating rate of 2 °C min^{-1}, but requires temperatures of more than 250 °C if the heating rate is increased to 10 °C min^{-1}. This behaviour indicates kinetic control for high heating rates, which implies that decomposition is a relatively slow process. Similar behaviour was observed for the decomposition of **1-Et** to give ZnO.[10] The TG curves recorded for the decomposition of **5-Me** to yield $Zn_{2.5}Co_{1.5}O_4$ are virtually identical to those recorded for **5-Et**.

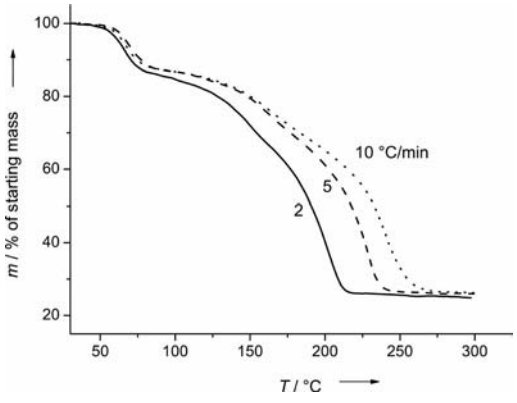

Figure 8. TG curves for **5** obtained at different heating rates (2, 5 and 10 °C min^{-1}).

The product of the decomposition is paramagnetic, as proven by SQUID measurements (see the Supporting Information). A typical powder diffractogram recorded after heating **5-Et** at a heating rate of 5 °C min^{-1} to an end temperature of 300 °C is displayed in Figure 9. The pattern can be explained by the presence of two phases, which are isostructural with ZnO (wurtzite phase) and CoO (cubic rock salt structure). From the differences in the line-broadening it can be directly concluded that the particles with a CoO-type phase are larger than those with a ZnO-type phase. The mean particle size was calculated by applying the Debye–Scherrer equation. For the phase isostructural with CoO, the particle size turned out to be around 48 nm (based on the peak at 2θ = 42.3°). The nanoparticles isostructural with wurtzite are significantly smaller, measuring 7.7 ± 0.4 nm (7.24 nm based on the peak at 2θ = 47.37° or 7.96 nm based on the peak at 2θ = 56.35°). The BET surface area is 37.2 m^2 g^{-1}, which gives an average particle size of 25 ± 1 nm. A representative TEM image is shown in Figure 10. It confirms the crystalline character of the nanoparticles. Finally, HAADF-STEM (high-angle annular dark-field scanning transmission electron microscopy) images of the mixed-oxide nanoparticles were recorded (see Figure 11). The profiles along two lines shown in Figure 11 indicate that both phases contain Zn and Co in varying molar ratios. It is well known that partial exchange of the Zn^{II} ions in wurtzite ZnO by Co^{II} ions is possible with vir-

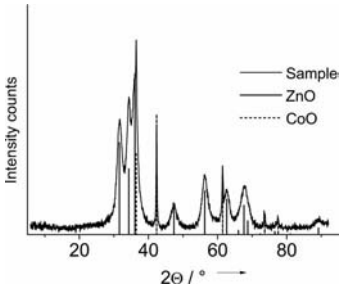

Figure 9. Powder diffractogramm obtained after the thermal decomposition of **5-Et** (end temperature 300 °C, 5 °C min^{-1} heating rate).

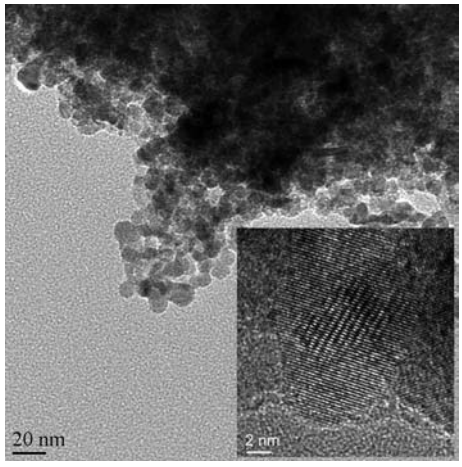

Figure 10. TEM image of the ZnO/CoO produced from **5-Et** (heating rate 5 °C min^{-1}). The inset shows a high-resolution image of the particles.

tually no change in the lattice parameters.[16] Similarly, solid solutions of Zn^{II} in a CoO lattice were reported, also with virtually no consequences on the lattice parameters.

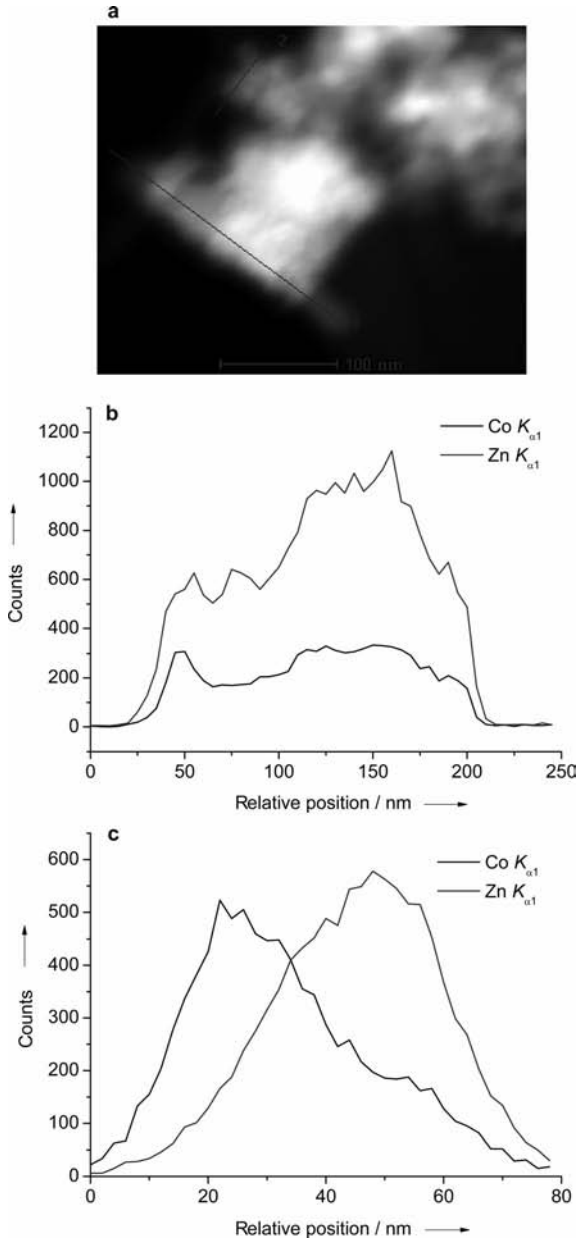

Figure 11. a) HAADF-STEM image of the mixed-oxide nanoparticles. The profiles along b) line 1 and c) line 2 reveal that both phases contain Zn and Co in different molar ratios.

Conclusions

Herein we have reported on the synthesis of tetra- and octanuclear mixed Zn/Co carbamate complexes using a new synthetic route. In this route a tetranuclear alkylzinc carbamate complex $[ZnR(O_2CR'_2)]_4$ is treated with a specially designed Co^{II} complex featuring pyridine ligands with additional secondary amino groups. These amino groups lead to cleavage of the tetrameric Zn carbamate complex and provide protons for alkane (RH) elimination. The product complexes $[(ZnR)_2M_2(O_2CNR'_2)_6]$ (M = Co or Zn in a molar ratio of 2.5:1.5) were subsequently used as single-source precursors for the fabrication of magnetic mixed-oxide nanoparticles under mild conditions ($T < 250$ °C). Analysis of the nanoparticles shows them to consist of two phases isostructural with ZnO (wurtzite phase) and CoO. The particles with a ZnO-type structure have an average size of 7.7 nm. The particles with a CoO-type structure are much larger (ca. 48 nm). Both phases contain Zn and Co in varying molar ratios. In future studies we will explore the possible applications of these mixed-oxide materials. This new method can presumably be applied to the synthesis of a variety of heterobimetallic carbamate complexes and precursors of mixed-oxide nanoparticles.

Experimental Section

General: All reactions were carried out using standard Schlenk techniques under N_2. All solvents were dried prior to use. UV/Vis spectra were recorded with a Varian CARY 5000 spectrometer. For the SQUID direct current (dc) measurements, a Quantum Design MPMS-XL 5 machine was used. Positive field desorption (FD^+) mass spectra were recorded with a JEOL JMS mass spectrometer. Elemental analyses were performed at the Microanalytical Laboratory of the University of Heidelberg. IR spectra were recorded with a Biorad Excalibur FTS3000 spectrometer. Thermogravimetric (TG) measurements were carried out with a Mettler TC15 under Ar in the range 30–300 °C. The heating rate was varied between 2 and 10 °C min^{-1}. Electron microscopy (TEM, STEM-HAADF, HRTEM) experiments and elemental analysis (EDX) were performed with a FEI Tecnai F20 ST TEM (operating voltage 200 kV) equipped with a field emission gun and EDAX EDS X-ray spectrometer [Si(Li) detecting unit, super ultra thin window, active area 30 mm^2, resolution 135 eV (at 5.9 keV)] on carbon-coated 400 mesh copper grids. The XRD measurements were performed with a STADI P machine from STOE and a Siemens D500 diffractometer using Cu radiation. The data were evaluated with EVA (DIFFRACplus, EVA 9.0, XRD evaluation programme, Bruker AXS, 2003). ICP measurements were performed on a Varian Liberty 150 AES apparatus. **1-Et** and **1-Me** were prepared as described in the literature.[10]

2: A solution of 2-(methylamino)pyridine (map; 0.148 g, 1.37 mmol) in CH_3OH (5 mL) was added to a CH_3OH solution (10 mL) of $CoCl_2$ (0.089 g, 0.685 mmol). The solution was stirred at 60 °C for 3 h. Then the solvent was removed in vacuo. Recrystallization from CH_3OH at room temp. afforded the product as blue crystals (0.159 g, 0.459 mmol, 67% yield). UV/Vis (toluene, $c = 2.85 \times 10^{-3}$ mol L^{-1}): $\tilde{\nu}$ (λ, ε) = 15640 (639, 86), 16100 (621, 83), 17100 (585 nm, 54 dm^3 mol^{-1} cm^{-1}) cm^{-1}. $C_{12}H_{16}Cl_2CoN_4$ (346.12): calcd. C 41.64, H 4.66, N 16.19; found C 41.04, H 4.60, N 15.95.

Crystal data for **2**: $C_{12}H_{16}Cl_2CoN_4$, M_r = 346.12, $0.60 \times 0.60 \times 0.55$ mm^3, monoclinic, space group $P2_1/c$, a = 12.732(3), b = 7.9800(16), c = 14.617(3) Å, β = 96.53(3)°, V = 1475.5(5) Å^3, Z = 4, $\rho_{calcd.}$ = 1.558 Mg m^{-3}, Mo-K_α radiation (graphite-monochromated, λ = 0.71073 Å), T = 100 K, θ_{range} = 1.61–30.03°. Reflections measured 24584, independent 4226, R_{int} = 0.0195. Final R indices [$I > 2\sigma(I)$]: R_1 = 0.0305, wR_2 = 0.0762.

3: A solution of 2-[2-(methylamino)ethyl]pyridine (maep; 0.74 g, 5.42 mmol) in CH_3OH (10 mL) was added to a CH_3OH solution

(40 mL) of $CoCl_2$ (0.705 g, 5.42 mmol). The solution was stirred at 60 °C for 3 h. The solution was then evaporated to dryness and the solid product recrystallized from CH_3OH at room temperature to give blue crystals (0.934 g, 65% yield). $C_8H_{12}Cl_2CoN_2$ (266.03): calcd. C 36.12, H 4.55, N 10.53; found C 36.15, H 4.47, N 10.64.

Crystal data for **3**: $C_8H_{12}Cl_2CoN_2$, M_r = 266.03, $0.35 \times 0.30 \times 0.30$ mm^3, monoclinic, space group $P2_1/c$, a = 12.681(3), b = 6.7560(14), c = 13.337(3) Å, b = 103.05(3)°, V = 1113.1(4) Å^3, Z = 4, $\rho_{calcd.}$ = 1.587 Mg m^{-3}, Mo-K_α radiation (graphite-monochromated, λ = 0.71073 Å), T = 100 K, θ_{range} = 3.14–30.00°. Reflections measured 7248, independent 3234, R_{int} = 0.0400. Final R indices [$I > 2\sigma(I)$]: R_1 = 0.0444, wR_2 = 0.1017.

4: A solution of 2-(2-methylaminoethyl)pyridine (maep; 0.618 g, 4.54 mmol) in CH_3OH (5 mL) was added to a CH_3OH solution (20 mL) of $CoCl_2$ (0.295 g, 2.27 mmol). The solution was stirred at 60 °C for 3 h. The solution was then evaporated to dryness and the solid product recrystallized from CH_3CN solution at room temperature to give pink crystals (0.599 g, 66%). $C_{16}H_{24}Cl_2CoN_4$ (402.23): calcd. C 47.78, H 6.01, N 13.93; found C 47.90, H 5.99, N 14.07.

Crystal data for **4**: $C_{16}H_{24}Cl_2CoN_4$, M_r = 402.22, $0.30 \times 0.20 \times 0.20$ mm^3, orthorhombic, space group $P2_1/n$, a = 9.998(2), b = 6.6600(13), c = 13.279(3) Å, V = 872.8(3) Å^3, Z = 2, $\rho_{calcd.}$ = 1.531 Mg m^{-3}, Mo-K_α radiation (graphite-monochromated, λ = 0.71073 Å), T = 100 K, θ_{range} = 2.38–30.00°. Reflections measured 5014, independent 2535, R_{int} = 0.0291. Final R indices [$I > 2\sigma(I)$]: R_1 = 0.0368, wR_2 = 0.0882.

5-Et: A solution of **2** (0.056 g, 0.162 mmol) in toluene (10 mL) was added to a toluene solution (5 mL) of **1-Et** (0.154 g, 0.162 mmol). The solution was stirred at 20 °C for 3 h. Then the solvent was removed in vacuo. Recrystallization from toluene at –20 °C afforded purple-coloured crystals of **5-Et**. Yield of crystalline product: 0.072 g (0.053 mmol, 33%). IR (CsI): $\tilde{\nu}$ = 1560 (s), 1493 (s) [ν(CO)], 1356 (s), 1163 (s), 1066 (m) [ν(CN)] cm^{-1}. UV/Vis (toluene, $c = 6.3 \times 10^{-3}$ mol L^{-1}): $\tilde{\nu}$ (λ, ε) = 16200 (617, 24), 16900 (592, 24), 18200 (549 nm, 16 dm^3 mol^{-1} cm^{-1}) cm^{-1}. $C_{58.8}H_{107}Cl_{0.6}Co_{1.5}N_6O_{12}Zn_{2.5}$ (1363.24): calcd. C 53.01, H 8.16, N 6.18; found C 52.47, H 8.35, N 6.62. AAS: Zn/Co ratio 2.5:1.5. ICP results: wt% Zn/Co ratio of 0.138:0.0783, corresponding to a molar ratio of Zn/Co of 2.45:1.55.

Crystal data for **5-Et**: $C_{58.80}H_{107}Cl_{0.60}Co_{1.5}N_6O_{12}Zn_{2.50}$, M_r = 1363.24, $0.30 \times 0.20 \times 0.20$ mm^3, triclinic, space group $P\bar{1}$, a = 12.191(2), b = 12.594(3), c = 13.095(3) Å, α = 116.34(3), β = 95.32(3), γ = 100.53(3)°, V = 1736.7(9) Å^3, Z = 1, $\rho_{calcd.}$ = 1.303 Mg m^{-3}, Mo-K_α radiation (graphite-monochromated, λ = 0.71073 Å), T = 100 K, θ_{range} = 1.73–27.43°. Reflections measured 14834, independent 7894, R_{int} = 0.0530. Final R indices [$I > 2\sigma(I)$]: R_1 = 0.0469, wR_2 = 0.0911.

5-Me: A solution of **2** (0.077 g, 0.222 mmol) in toluene (10 mL) was added to a toluene solution (5 mL) of **1-Me** (0.2 g, 0.222 mmol). The solution was stirred at 20 °C for 3 h. The solution was then evaporated to dryness and the solid product recrystallized from toluene at –20 °C to give purple crystals of **5-Me**. Yield of crystalline product: 0.094 g (0.071 mmol, 32%). IR (CsI): $\tilde{\nu}$ = 2984 (m), 2874 (w) [ν(CH)], 1565 (s), 1498 (s) [ν(CO)], 1354 (s), 1153 (s), 1074 (m) [ν(CN)] cm^{-1}. UV/Vis (toluene, $c = 7.6 \times 10^{-3}$ mol L^{-1}): $\tilde{\nu}$ (λ, ε) = 17000 (588, 17), 19120 (523, 9), 21050 (475 nm, 2 dm^3 mol^{-1} cm^{-1}) cm^{-1}. $C_{43.3}H_{87.6}Cl_{0.6}Co_{1.5}N_6O_{12}Zn_{2.5}$·$C_7H_8$ (1251.99): calcd. C 51.82, H 8.02, N 6.31; found C 51.05, H 7.81, N 6.41.

Crystal data for **5-Me**: $C_{100.70}H_{191.10}Cl_{1.30}Co_3N_{12}O_{24}Zn_5$, M_r = 2503.98, $0.30 \times 0.25 \times 0.25$ mm^3, triclinic, space group $P\bar{1}$, a = 14.013(3), b = 15.536(3), c = 17.012(3) Å, α = 76.49(3), β = 77.96(3), γ = 74.98(3)°, V = 3434.6(12) Å^3, Z = 2, $\rho_{calcd.}$ = 1.211 Mg m^{-3}, Mo-K_α radiation (graphite-monochromated, λ = 0.71073 Å), T = 100 K, θ_{range} = 2.27–29.16°. Reflections measured 34158, independent 18347, R_{int} = 0.0226. Final R indices [$I > 2\sigma(I)$]: R_1 = 0.0443, wR_2 = 0.1297.

6: The new carbamate complex **6** crystallized from a solution of **5-Et** (0.011 g) in CH_3CN (2 mL). IR (CsI): $\tilde{\nu}$ = 2955 (m), 2892 (w) [ν(CH)], 1573 (s), 1474 (s) [ν(CO)], 1345 (s), 1212 (s), 1159 (s), 1072 (m) [ν(CN)] cm^{-1}. UV/Vis (toluene, $c = 1.86 \times 10^{-2}$ mol L^{-1}): $\tilde{\nu}$ (λ, ε) = 16050 (623, 27), 17000 (589, 26), 18380 (544 nm, 18 dm^3 mol^{-1} cm^{-1}) cm^{-1}. MS (FD$^+$, toluene, $c = 1 \times 10^{-3}$ mol L^{-1}): calcd. for $[Zn_2Co_2(\mu_4\text{-}O)\{O_2CN(i\text{Pr})_2\}_6]$ 1182.36; found 1182.40; calcd. for $[Zn_3Co(\mu_4\text{-}O)\{O_2CN(i\text{Pr})_2\}_6]$ 1187.35; found 1187.39. $C_{42}H_{84}Co_{1.5}N_6O_{13}Zn_{2.5}$·$2CH_3CN$ (1215.08): calcd. C 46.62, H 7.56, N 7.10; found C 41.09, H 6.91, N 6.98.

Crystal data for **6**: $C_{92}H_{180}Co_3N_{16}O_{26}Zn_5$, M_r = 2430.16, $0.35 \times 0.30 \times 0.30$ mm^3, monoclinic, space group $P2_1/c$, a = 14.321(3), b = 35.817(7), c = 24.108(5) Å, β = 99.44(3)°, V = 12198(4) Å^3, Z = 4, $\rho_{calcd.}$ = 1.323 Mg m^{-3}, Mo-K_α radiation (graphite-monochromated, λ = 0.71073 Å), T = 100 K, θ_{range} = 1.42–30.00°. Reflections measured 71386, independent 35552, R_{int} = 0.0806. Final R indices [$I > 2\sigma(I)$]: R_1 = 0.0608, wR_2 = 0.1309.

7: Complex **7** crystallized from a solution of **5-Et** (0.012 g) in hexane (2 mL). IR (solid CsI): $\tilde{\nu}$ = 2963 (m), 2889 (w) [ν(CH)], 1566 (s), 1466 (s) [ν(CO)], 1358 (s), 1219 (s), 1165 (s), 1066 (s) [ν(CN)] cm^{-1}. UV/Vis (toluene, $c = 1.95 \times 10^{-2}$ mol L^{-1}): $\tilde{\nu}$ (λ, ε) = 16050 (623, 25), 17010 (588, 24), 18350 (545, 16) cm^{-1}. $C_{92}H_{177}Co_3N_6O_{26}Zn_5$ (2287.13): calcd. C 46.65, H 7.56, N 7.10; found C 42.44, H 7.34, N 6.17. AAS: Zn/Co ratio 5:3. ICP results: wt% in sample Zn/Co ratio of 0.228:0.108, corresponding to a molar ratio of Zn/Co of 5.17:2.83.

Crystal data for **7**: $C_{92.20}H_{177.40}N_{12}O_{26}Co_3Zn_5$, M_r = 4747.80, $0.25 \times 0.25 \times 0.20$ mm^3, triclinic, space group $P\bar{1}$, a = 15.062(3), b = 15.173(3), c = 15.893(3) Å, α = 65.93(3), β = 67.16(3), γ = 88.02(3)°, V = 3022.9(10) Å^3, Z = 1, $\rho_{calcd.}$ = 1.304 Mg m^{-3}, Mo-K_α radiation (graphite-monochromated, λ = 0.71073 Å), T = 100 K, θ_{range} = 1.54–27.50°. Reflections measured 25184, independent 13616, R_{int} = 0.0700. Final R indices [$I > 2\sigma(I)$]: R_1 = 0.1072, wR_2 = 0.3283.

Synthesis of Oxide Nanoparticles from 5-Et: Complex **5-Et** (0.014 g, 0.010 mmol) was placed in a platinum crucible. The compound was heated at different heating rates (2, 5 and 10 °C min^{-1}) under N_2 with a flow rate of 150 mL min^{-1}. The starting temperature was settled at 30 °C and the end temperature was fixed at 300 °C. Decomposition of the mixed Zn/Co carbamate led to the formation of 0.0034 g of Zn/Co oxide nanoparticles. BET surface area: 37.2 m^2 g^{-1}; average particle size: 25 ± 1 nm. Powder X-ray diffraction analysis: CoO mean particle size: 47.7 ± 0.3 nm; ZnO mean particle size: 7.7 ± 0.4 nm.

X-ray Crystallographic Study: Suitable crystals were taken directly out of the mother liquor, immersed in perfluorinated polyether oil and fixed on top of a glass capillary. Measurements were made with a Nonius-Kappa CCD diffractometer with a low-temperature unit using graphite-monochromated Mo-K_α radiation. The temperature was set to 100 K. The data collected were processed using the standard Nonius software.[26] All calculations were performed using the SHELXT-PLUS software package. Structures were solved by direct methods with the SHELXS-97 program and refined with the SHELXL-97 program.[27,28] Graphical handling of the structural data during solution and refinement was performed

with XPMA.[29] Atomic coordinates and anisotropic thermal parameters of non-hydrogen atoms were refined by full-matrix least-squares calculations.

CCDC-796027 (for **2**), -796029 (for **3**), -796028 (for **4**), -796030 (for **5-Me**), -796031 (for **5-Et**), -796033 (for **6**) and -796032 (for **7**) contain contains the supplementary crystallographic data for this paper. These data can be obtained free of charge from The Cambridge Crystallographic Data Centre via www.ccdc.cam.ac.uk/data_request/cif.

Supporting Information (see the footnote on the first page of this article): Photo showing solid **5-Et**, EDX data for the Zn/Co oxide particles, χT vs. T curve as derived from the SQUID measurements (500 Oe) for the Co/Zn oxide particles.

Acknowledgments

We thank Prof. Dr. Wolfgang Scherer (Universität Augsburg) for fruitful discussions. Continued financial support from the Deutsche Forschungsgemeinschaft (DFG) is gratefully acknowledged.

[1] M. L. Kahn, A. Glaria, C. Pages, M. Monge, L. S. Macary, A. Maisonnat, B. Chaudret, *J. Mater. Chem.* **2009**, *19*, 4044–4060, and references therein.
[2] Q. Zhang, C. S. Dandeneau, X. Zhou, G. Cao, *Adv. Mater.* **2009**, *21*, 4087–4108.
[3] K. Keis, E. Magnusson, H. Lindstrom, S. E. Lindquist, A. Hagfeldt, *Sol. Energy Mater. Sol. Cells* **2002**, *73*, 51–58.
[4] A. B. F. Martinson, T. W. Hamann, M. J. Pellin, J. T. Hupp, *Chem. Eur. J.* **2008**, *14*, 4458–4467.
[5] Q. Zhang, T. P. Chou, B. Russi, S. A. Jenekhe, G. Cao, *Angew. Chem.* **2008**, *120*, 2436; *Angew. Chem. Int. Ed.* **2008**, *47*, 2402–2406.
[6] M. Monge, M. L. Kahn, A. Maisonnat, B. Chaudret, *Angew. Chem.* **2003**, *115*, 5479–5482; *Angew. Chem. Int. Ed.* **2003**, *42*, 5321–5324.
[7] a) M. L. Kahn, M. Monge, V. Colliere, F. Senocq, A. Maisonnat, B. Chaudret, *Adv. Funct. Mater.* **2005**, *15*, 458–468; b) M. L. Kahn, M. Monge, E. Snoeck, A. Maisonnat, B. Chauret, *Small* **2005**, *1*, 221–224; c) M. L. Kahn, T. Cardinal, B. Bousquet, M. Monge, V. Jubera, B. Chauret, *ChemPhysChem* **2006**, *7*, 2392–2397.
[8] a) A. Roy, S. Polarz, S. Rabe, B. Rellinghaus, H. Zahres, F. E. Kruis, M. Driess, *Chem. Eur. J.* **2004**, *10*, 1565–1575; b) S. Polarz, A. Roy, M. Merz, S. Halm, D. Schröder, L. Scheider, G. Bacher, F. E. Kruis, M. Driess, *Small* **2005**, *1*, 540–552; c) S. Polarz, F. Neues, M. Van der Berg, W. Grünert, L. Khodeir, *J. Am. Chem. Soc.* **2005**, *127*, 12028–12034; d) V. Ischenko, S. Polarz, D. Grote, V. Stavarache, K. Fink, M. Driess, *Adv. Funct. Mater.* **2005**, *15*, 1945–1954; e) S. Polarz, J. Strunk, V. Ischenko, M. Van der Berg, O. Hinrichsen, M. Muhler, M. Driess, *Angew. Chem.* **2006**, *118*, 3031–3035; *Angew. Chem. Int. Ed.* **2006**, *45*, 2965–2969; f) M. Van der Berg, S. Polarz, O. P. Tkachenko, K. V. Klementiev, M. Bandyopadhyay, L. Khodeir, H. Gies, M. Muhler, W. Grünert, *J. Catal.* **2006**, *241*, 446–455; g) S. Polarz, A. Roy, M. Lehmann, M. Driess, F. E. Kruis, A. Hoffmann, P. Zimmer, *Adv. Funct. Mater.* **2007**, *17*, 1385–1391; h) S. Polarz, A. Orlov, F. Schüth, A. H. Lu, *Chem. Eur. J.* **2007**, *13*, 592–597; i) A. Orlov, A. Roy, M. Lehmann, M. Driess, S. Polarz, *J. Am. Chem. Soc.* **2007**, *129*, 371–375; j) C. Lizandara-Pueyo, M. W. E. van den Berg, A. De Toni, T. Goes, S. Polarz, *J. Am. Chem. Soc.* **2008**, *130*, 16601–16610.
[9] S. Polarz, A. V. Orlov, M. W. E. Van den Berg, M. Driess, *Angew. Chem.* **2005**, *117*, 8104–8109; *Angew. Chem. Int. Ed.* **2005**, *44*, 7892–7896.
[10] D. Domide, E. Kaifer, J. Mautz, O. Walter, S. Behrens, H.-J. Himmel, *Eur. J. Inorg. Chem.* **2008**, 3177–3185.
[11] A. J. Petrella, H. Deng, N. K. Roberts, R. N. Lamb, *Chem. Mater.* **2002**, *14*, 4339–4342.
[12] a) M. R. Hill, P. Jensen, J. J. Russell, R. N. Lamb, *Dalton Trans.* **2008**, 2751–2758; b) M. R. Hill, J. J. Russell, R. N. Lamb, *Chem. Mater.* **2008**, *20*, 2461–2467.
[13] H. Falk, J. Hübner, P. J. Klar, W. Heimbrodt, *Phys. Rev. B* **2003**, *68*, 165203-1-12.
[14] Z. Xiao, H. Matsui, N. Hasuike, H. Harima, H. Tabata, *J. Appl. Phys.* **2008**, *103*, 043504–1–5.
[15] M. Snure, D. Kumar, A. Tiwari, *JOM* **2009**, *61*, 72–75.
[16] L. Poul, S. Ammar, N. Jouini, F. Fiévet, F. Villain, *Solid State Sci.* **2001**, *3*, 31–42.
[17] For mechanistic studies using quantum chemical calculations, see: H.-J. Himmel, *Eur. J. Inorg. Chem.* **2007**, 675–683.
[18] D. Domide, C. Neuhäuser, E. Kaifer, H. Wadepohl, H.-J. Himmel, *Eur. J. Inorg. Chem.* **2009**, 2170–2178.
[19] C. Neuhäuser, D. Domide, J. Mautz, E. Kaifer, H.-J. Himmel, *Dalton Trans.* **2008**, 1821–1824.
[20] Y. Tang, W. S. Kassel, L. N. Zakharov, A. L. Rheingold, R. A. Kemp, *Inorg. Chem.* **2005**, *44*, 359–264.
[21] D. B. Dell'Amico, F. Calderazzo, B. Giovannitti, G. Pelizzi, *J. Chem. Soc., Dalton Trans.* **1984**, 647–652.
[22] We observed the formation of the complex $[(map)_2ZnCl_2]$ as a side-product in the course of the reaction of **2** with both **1-Et** and **1-Me**.
[23] A. Belforte, F. Calderazzo, U. Englert, J. Strähle, *Inorg. Chem.* **1991**, *30*, 3778–3781.
[24] M. Casarin, E. Tondello, F. Calderazzo, A. Vittadini, M. Bettinelli, A. Gulino, *J. Chem. Soc. Faraday Trans.* **1993**, *89*, 4363–4367.
[25] P. F. Haywood, M. R. Hill, N. K. Roberts, D. C. Craig, J. J. Russell, R. N. Lamb, *Eur. J. Inorg. Chem.* **2008**, 2024–2032.
[26] *DENZO-SMN, Data processing software*, Nonius, **1998** (http://www.nonius.com).
[27] a) G. M. Sheldrick, *SHELXS-97*, *Program for Crystal Structure Solution*, University of Göttingen, Göttingen, **1997** (http://shelx.uni-ac.gwdg.de/SHELX/index.html); b) G. M. Sheldrick, *SHELXL-97*, *Program for Crystal Structure Refinement*, University of Göttingen, Göttingen, **1997** (http://shelx.uni-ac.gwdg.de/SHELX/index.html).
[28] *International Tables for X-ray Crystallography*, vol. 4, Kynoch Press, Birmingham, **1974**.
[29] L. Zsolnai, G. Huttner, *XPMA*, University of Heidelberg, Heidelberg, **1994** (http://www.uni-heidelberg.de/institute/fak12/AC/huttner/software/software.html).

Received: October 14, 2010
Published Online: January 17, 2011

